PSO-based MPPT control of wind-driven Self-Excited Induction Generator for pumping system

Mohamed. Ali Zeddini, Remus Pusca, Anis Sakly, M. Faouzi Mimouni

PSO-based MPPT Control of Wind-driven Self-Excited Induction Generator for Pumping System

Mohamed. Ali Zeddini [1], Remus Pusca [2], Anis Sakly [1], M. Faouzi Mimouni [1]

(1) Research unit: Industrial Systems Study and Renewable Energy (ESIER), National Engineering School of Monastir (ENIM), University of Monastir, Tunisia.

(2) Artois University, EA4025, Laboratory of Electrical Systems and Environment (LSEE), Bethune, F-62400, France.

zeddini_med_ali_enim@yahoo.fr

Abstract

In recent years, much research has been done to improve the performance of a wind energy conversion system at various wind speeds using **M**aximum **P**ower **P**oint **T**racking (**MPPT**) algorithms to find an efficient production of peak energy.

In most cases, the MPPT techniques used to maximize the turbines power coefficient neglect the effect of losses generated by the system components, which can shift the true optimal operating point of the wind turbine. Furthermore, conventional MPPT methods such as **P**erturbation and **O**bservation (**P&O**) and **I**ncremental of **C**onductance (**IncCond**), need to sense both the rotor speed and the power of the wind turbine. In addition, other methods such as Fuzzy Logic and neural networks based on MPPT algorithms are proposed but these methods require knowledge of the wind speed and system parameters for the training phase.

In this context, a new MPPT technique is being proposed in this paper, based on **P**article **S**warm **O**ptimization (**PSO**) for a standalone **S**elf-**E**xcited **I**nduction **G**enerator (**SEIG**) operating at variable wind speed and supplying an induction motor coupled to a centrifugal pump.

Keywords - Self Excited Induction Generator, Pumping system, Maximum Power Point Tracking Particle Swarm Optimization

1. Introduction

In the last decades, producing electricity with renewable energies such as wind and solar energy has been considered to replace conventional resources [1-3]. Particularly, in remote site it is important to limit the maintenance and to operate with minimum storage batteries, so the wind turbine pumping systems without energy storage can be an alternative solution to conventional powered pumping systems. In addition, this type of pumping systems does not pollute the environment.

Many types of generators are used for stand-alone power generation in remote site such as permanent magnet, brushless, synchronous, asynchronous, variable reluctance. But the **S**elf **E**xcited **I**nduction **G**enerator (**SEIG**) is mainly used because of its lower cost, high power density and very little maintenance required [4-6].

During the last decades, several works have been developed to investigating a performance analysis of the SEIG, and dynamic performance for feeding static and dynamic loads (resistive, inductive, capacitive, and induction motor) at various wind speed conditions [7-10]. Therefore, the power converter topology have been developed and various regulating schemes explored to obtain improved voltage and frequency regulation [11,12]. In this scheme, the SEIG needs to control the providing bidirectional flow of both active and reactive powers.

Other works have focused on architectures and methods for maximizing the wind power. Among them, various regulating schemes have been adopted to extract the maximum power from the wind turbine [13-15]. Consequently, the SEIG is operating at variable frequency, which needs a single power controller. However, this scheme is gaining importance for stand-alone wind power applications, in particular for water pumping systems with **I**nduction **M**otor (**IM)** where the variation of the electrical parameters is not very critical for its use.

Indeed, different control strategies referred to **M**aximum **P**ower **P**oint **T**racking (**MPPT)** algorithms are used to track peak power production efficiently at varying wind speeds. In this context, many techniques of MPPT controller have been applied to induction generators such as, **P**erturb and **O**bserve (**P&O**) or Fuzzy logic, Neural network estimator [16-20]. The P&O technique is often proposed as solution for MPPT controller for its simplicity calculus algorithm. The disadvantage of this technique is that it introduces a continuous oscillation around the real maximum power point and have a limited ability to track this point in the transient environmental conditions [16,17]. As a solution to improve the tracking algorithm under speed-varying changes in wind speed, the Adaptive step Perturb and Observe strategy is proposed in [18,19]. However, this technique which minimizes the oscillation needs to use the generator rotor speed variation (as complementary information) to provide the correct direction to the **M**aximum **P**ower **P**oint (**MPP**).

Other MPPT strategies are implemented using intelligent computations like Artificial Neural Networks [20] and Fuzzy logic [21, 22]. Recent improvements using a Fuzzy-Neuro based algorithm, combined with an additional measurement of wind speed, obtain excellent precision in the tracking, but increase the computational burden and cost.

In this context, this paper presents a PSO-MPPT controller of wind-driven Self-Excited Induction Generator for pumping systems which have not need to measure the wind or turbine speed. A SEIG-Pump performance analysis is developed to extract the maximum power rated from the wind turbine. The frequency is reached by using a **T**hyristor **C**ontroller **R**eactor (**TCR**) to adapt the rotor speed of the SEIG at the desired value.

The whole paper is organized as follows: section 2 describes the dynamic modeling of the SEIG pumping system, section 3 is devoted to presents the principle of MPPT control strategies. Simulation results performed with Matlab/Simulink are discussed and presented in section 4. The location of the MPP is calculated for different wind speed values to show the robustness and the efficiency of the

propose **PSO MPPT** algorithm. Experimental results are presented in section 5 with measurements on a test bench wind turbine emulator. Finally, a conclusion sums up the developed work and its features.

2. Modeling of Wind Turbine Conversion System

A wind turbine energy conversion system intended to work in isolated sites is shown in Fig.1. It consists of a DC Motor controlled through a chopper to emulate the wind turbine model used to convert wind kinetic energy , a squirrel cage **I**nduction **G**enerator (**IG**) to convert the mechanical power provided from the DC motor on electrical power, an induction motor which is coupled with a mechanical break to emulate the centrifugal pump model, a frequency controller based on Thyristor Controller Reactor system which is used to locate the MPP from the wind turbine, and a dSPACE controller board which is interfaced with a PC under Matlab/Simulink for the implementation of the PSO-MPPT controller .

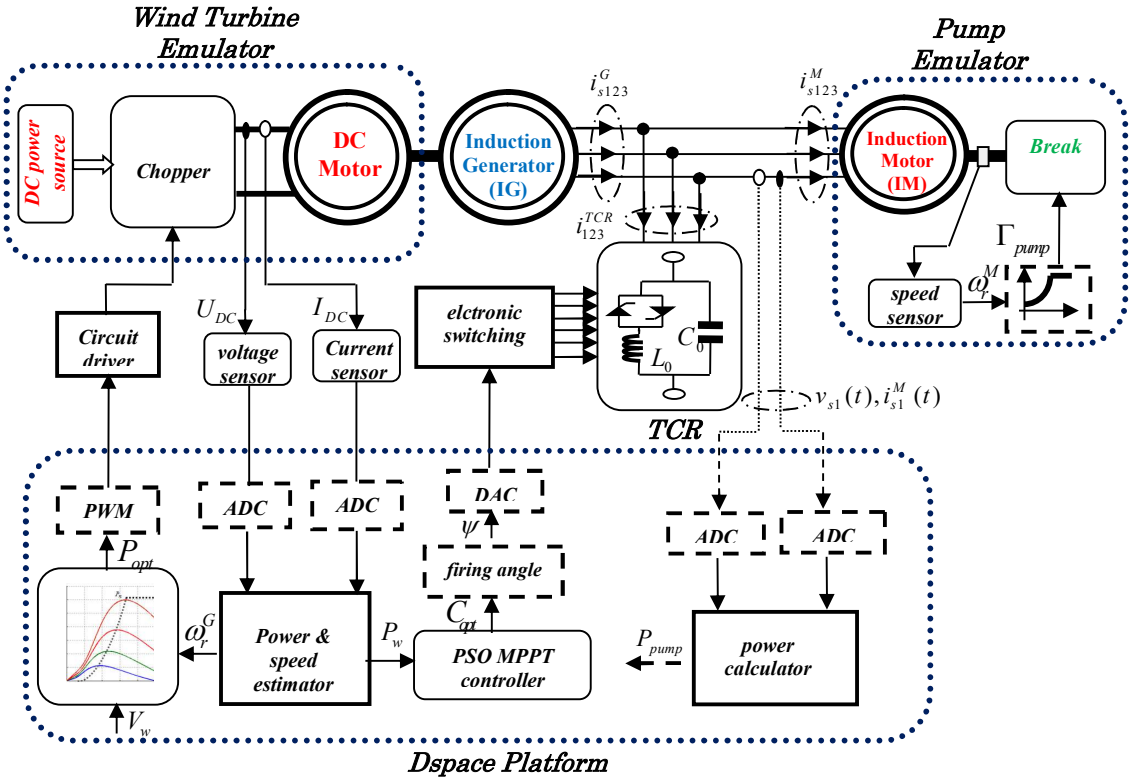

Fig .1. Schematic block diagram of the experimental test-bench of the wind turbine energy conversion system.

2.1. Modeling of Wind Turbines Curve

The power delivered by the wind turbine is proportional to the cube of the wind speed and can be expressed as:

$$P_w = \frac{1}{2}\rho A V_w^3 \tag{1}$$

where ρ is the air density, A is the area swept by blades and V_w is the wind speed. A wind turbine can only extract part of the power (maximum 59%) from the wind, which is given by the Betz limit [23]. Therefore, the wind turbine mechanical power extracted from the wind is given by:

$$P_m = \frac{1}{2}\rho A C_p(\beta,\lambda) V_w^3 \tag{2}$$

where $C_p(\lambda,\beta)$ is the power coefficient of the wind turbine. In this paper, the value of $C_p(\lambda,\beta)$ is calculated as follows [24]:

$$C_p(\lambda,\beta) = 0.5179(116\lambda_i - 0.4\beta + 5)e^{-21\lambda_i} + 0.068\lambda \tag{3}$$

where the parameter λ_i is expressed as:

$$\lambda_i = \frac{1}{0.5/(\lambda + 0.08\beta) - 0.035/(\beta^2 + 1)} \tag{4}$$

The Tip Speed Ratio (TSR) is defined as the ratio between the blade tip speed and the wind speed:

$$\lambda = \frac{R_w \Omega_r}{V_w} \tag{5}$$

where Ω_r denotes the rotor speed, and R_w is the radius of the wind turbine blade. The torque developed by the wind turbine is given by:

$$\Gamma_w = \frac{P_m}{\Omega_r} = \frac{R_w}{2\lambda}\rho A V_w^2 C_p(\beta,\lambda) \tag{6}$$

β is the blade pitch angle, and λ is the Tip Speed Ratio.

Fig. 2 shows the power coefficient and the mechanical power curves of the wind turbine as a function of the rotor speed for a pitch angle $\beta = 0°$.

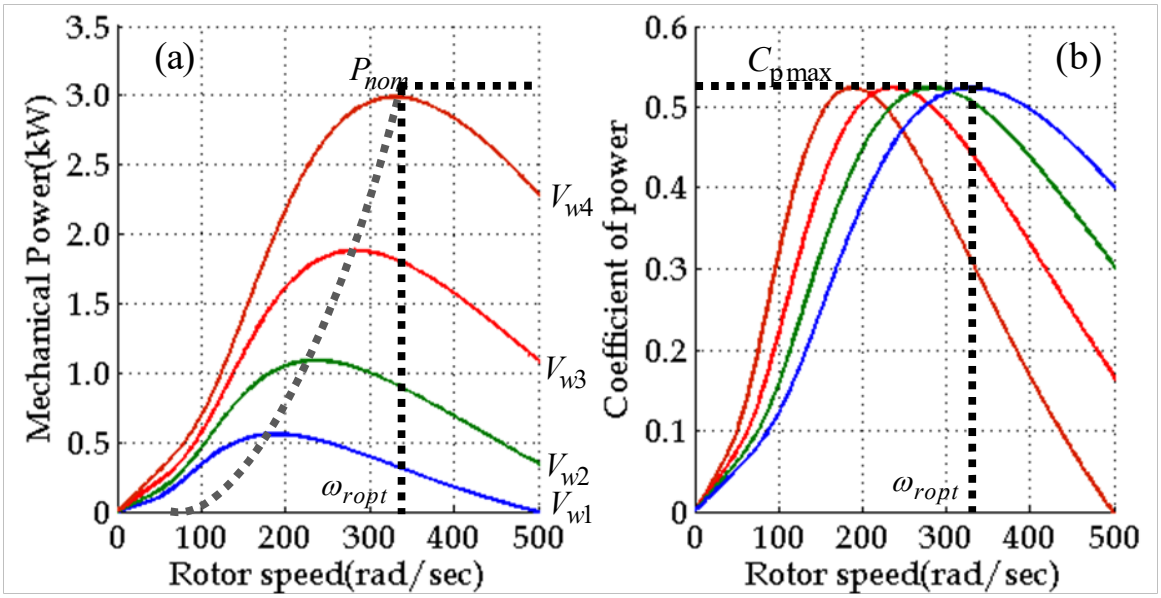

Fig. 2 Variation of (a) mechanical power curves and (b) power coefficient of the wind turbine for different wind speeds.

2.2. Modeling of the Self Excited Induction Generator

For the modeling and analysis of the SEIG, the stationary reference frame model is used. Moreover, the following differential equations describing the global generator model including the IG currents ($i_{sd}^{G}, i_{sq}^{G}, i_{rd}^{G}, i_{rq}^{G}$) which integrated the auto-excitement capacitor C and the IM currents (i_{sd}^{M}, i_{sq}^{M}) are developed as:

$$\frac{d}{dt}\begin{pmatrix} i_{sd}^{G} \\ i_{sq}^{G} \\ i_{rd}^{G} \\ i_{rq}^{G} \\ v_{sd} \\ v_{sd} \end{pmatrix} = \frac{1}{D^{G}}\left\{ \begin{bmatrix} L_r^G R_s^G & -L_m^{G^2}\omega_r^G & -L_m^G R_r^G & -L_m^G L_r^G \omega_r^G & -L_r^G & 0 \\ L_m^{G^2}\omega_r^G & L_r^G R_s^G & L_m^G L_r^G \omega_r^G & -L_m^G R_r^G & 0 & -L_r^G \\ -L_m^G R_s^G & L_m^G L_s^G \omega_r^G & L_s^G R_r^G & L_s^G L_r^G \omega_r^G & L_m^G & 0 \\ -L_m^G L_s^G \omega_r^G & -L_m^G R_s^G & -L_s^G L_r^G \omega_r^G & L_s^G R_r^G & 0 & L_m^G \\ \frac{1}{C} & 0 & 0 & 0 & \frac{1}{C} & 0 \\ 0 & \frac{1}{C} & 0 & 0 & 0 & \frac{1}{C} \end{bmatrix} \begin{pmatrix} i_{sd}^{G} \\ i_{sq}^{G} \\ i_{rd}^{G} \\ i_{rq}^{G} \\ i_{sd}^{M} \\ i_{sq}^{M} \end{pmatrix} - \omega_r^G \begin{pmatrix} -L_m^G \\ -L_m^G \\ L_s^G \\ L_s^G \end{pmatrix} \phi_0 \right\} \quad (7)$$

where, $L_s^G = l_s^G + L_m^G$ $L_r^G = l_r^G + L_m^G$, and $D^G = L_m^{G^2} - L_s^G L_r^G$

R_s^G is the winding stator resistance, R_r^G the rotor resistance and ω_r^G the rotor speed of the wind induction generator.

118 ϕ_0 is the remanant of the residual flux linkages, l_s^G the leakage inductance of the stator winding, l_r^G
119 leakage inductance of the rotor copper arrangement referred to the stator, and L_m^G magnetizing
120 inductance of the IG.
121 The electromagnetic torque developed by the IG can be computed in $d-q$ axes stator and rotor currents
122 as:

123 $$\Gamma_{em}^G = \frac{3}{2}\left(\frac{p}{2}\right)\left[i_{rd}^G i_{sq}^G - i_{sd}^G i_{rq}^G\right] \tag{8}$$

124 The equation which represents the SEIG mechanical behavior will be assumed to be expressible as:

125 $$\begin{cases} J\dfrac{d\Omega_r^G}{dt} + \Gamma_f = \Gamma_\omega - \Gamma_{em}^G \\ \Gamma_\omega = \dfrac{P_w}{\Omega_r^G} \end{cases} \tag{9}$$

126 where Γ_w represents the torque which acts on the SEIG shaft by means of the blades, Γ_f is the friction
127 torque, P_w is the corresponding mechanical power and J is the global inertia of the system.

128 **2.3. Model of the Induction Motor**

129 The differential equations describing the stator currents (i_{sd}^M , i_{sq}^M) and rotor currents (i_{rd}^M and i_{rq}^M) of
130 the IM using a $d-q$ components of stator voltage (v_{sd} and v_{sq}) are developed as:

131 $$\frac{d}{dt}\begin{pmatrix} i_{sd}^M \\ i_{sq}^M \\ i_{rd}^M \\ i_{rq}^M \end{pmatrix} = \frac{1}{D^M}\begin{bmatrix} -pL_m^M\ \Omega_r^M & -L_r^M r_s^M & -pL_m^M L_r^M \Omega_r^M & -L_m^M r_r^M \\ -L_r^M r_s^M & pL_m^{M\,2}\Omega_r^M & -L_m^M r_r^M & pL_m^M L_r^M \Omega_r^M \\ pL_m^M L_s^M \Omega_r^M & L_m^M r_s^M & pL_s^M L_r^M \Omega_r^M & L_s^M r_r^M \\ L_m^M r_s^M & -pL_m^M L_s^M \Omega_r^M & L_s^M r_r^M & pL_s^M L_r^M \Omega_r^M \end{bmatrix}\begin{pmatrix} i_{sd}^M \\ i_{sq}^M \\ i_{rd}^M \\ i_{rq}^M \end{pmatrix} + \frac{1}{D^M}\begin{bmatrix} -L_r^M & 0 \\ 0 & -L_r^M \\ L_m^M & 0 \\ 0 & L_m^M \end{bmatrix}\begin{pmatrix} v_{sd} \\ v_{sq} \end{pmatrix} \tag{10}$$

132 where, $L_s^M = l_s^M + L_m^M$ $L_r^M = l_r^M + L_m^M$ and $D^M = L_m^{M^2} - L_s^M L_r^M$,

l_s^M is the leakage inductance of the stator winding, l_r^M leakage inductance of the rotor copper arrangement referred to the stator and p is the pair of poles. r_s^M is the winding stator resistance, r_r^M the rotor resistance and ω_r^M the rotor speed of the induction motor.

The electromagnetic torque of the IM can be computed in $d-q$ axes stator and rotor currents as:

$$\Gamma_{em}^M = \frac{3}{2}\left(\frac{p}{2}\right)\left[i_{rd}^M i_{sq}^M - i_{sd}^M i_{rq}^M\right] \tag{11}$$

The equation which represents the IM mechanical behavior will be expressible as:

$$\begin{cases} J\dfrac{d\Omega_r^M}{dt} + \Gamma_f = \Gamma_{em}^G - \Gamma_{pump} \\ \Gamma_{pump} = \dfrac{P_{pum}}{\Omega_r^M} = k_n \Omega_r^{M^2} \end{cases} \tag{12}$$

with k_n …..and P_{pump} electrical pump power

2.4. Modeling of the TCR System

A **T**hyristor **C**ontrolled **R**eactor circuit is basically composed of two oppositely poled thyristors and a reactor [25,8]. The reactor is composed as two elements; a relatively big fixed capacitor $C_0 = 75\ \mu F$ and a fixed self inductance $L_0 = 335$ mH. A per phase circuit of TCR circuit is shown in Fig. 3.

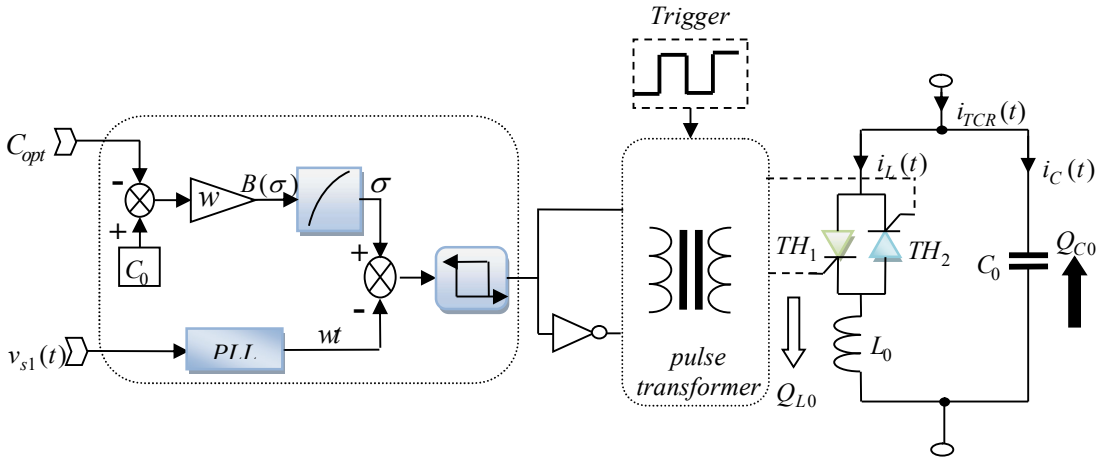

Fig. 3. Per phase equivalent circuit of TCR system and open loop control scheme for frequency regulation.

148 The instantaneous current absorbed by the self inductance L_0 is given by:

149
$$i_{L0} = \begin{cases} \dfrac{V_s}{\pi . L_0 \omega}\sqrt{2}[\cos(\psi) - \cos(\omega . t)] & \psi < \omega . t < \psi + \sigma \\ 0 & \psi + \sigma < \omega . t < \pi \end{cases} \quad (13)$$

150 where σ is the thyristor conduction angle, and ψ is the thyristor firing angle.

151 V_s and ω are the RMS and the frequency of the SEIG terminal voltage respectively.

152 The fundamental component is found by Fourier analysis, and is given by:

153
$$I_1 = \frac{\sigma - \sin(\sigma)}{\pi L_0 \omega} V_s = B(\sigma) V_s \quad (14)$$

154 where $B(\sigma)$ is an adjustable fundamental frequency susceptance.

155 The TCR system is controlled by adjusting a fundamental frequency susceptance whose reactive
156 power is balanced according to the requirement current in the SEIG. However, the reactive power Q_{TCR}
157 generated by a TCR system is equal to the difference between the capacitor power Q_{C0} and the
158 inductance power Q_L as:

159
$$Q_{TCR} = Q_{C0} - Q_{L0} = 3(C_0 \omega - B(\sigma)) V_s^2 \quad (15)$$

160 The generated firing pulses for the thyristors are obtained by a pulse transformer and a trigger which
161 is synchronized with the line voltages using a PLL system.

162 **3. Analysis of the Proposed MPPT Controller**

163 **3.1. MPPT Controller Principle**

164 Considering the mechanical power curves presented in Fig. 2.a we can note that the power of a wind
165 turbine is maximum for a rotor speed called optimum rotor speed ω_{ropt} . So in order to extract maximum

166 possible power, the wind turbine aloud be operates at this speed. During the constant wind speed is
167 possible to control the rotational speed of the wind turbine by changing the reactive power.

168 Note that the operating slip of the induction generator is a small value. Therefore, for operating at
169 **M**aximum **P**ower **P**oint (**MPP**), the rotor speed can be controlled by adjusting the capacitor value which
170 also influences the frequency value of the SEIG. In a classical P&O algorithm, the MPP can be obtained
171 by measuring two parameters: electrical power (P_w) and rotor speed ω_r . The particularity of the
172 proposed PSO algorithm is that it uses only electrical power (P_w) parameter as reference to estimate the
173 optimal value of the capacitor which lead to ω_{ropt} .

174 For the wind turbine emulation, the proposed PSO-MPPT controller is based on measurement of
175 electrical variables (U_{DC} and I_{DC}) as is shown in Fig. 4a. In a real wind turbine, the measurement of the
176 mechanical power is complex or not always available. So it is possible to maximize the electrical power
177 extracted from the SEIG considering the measured power at the SEIG output as the image of the
178 mechanical power at the SEIG shaft. This case is shown in Fig. 4b and proposed in the presented PSO
179 algorithm.

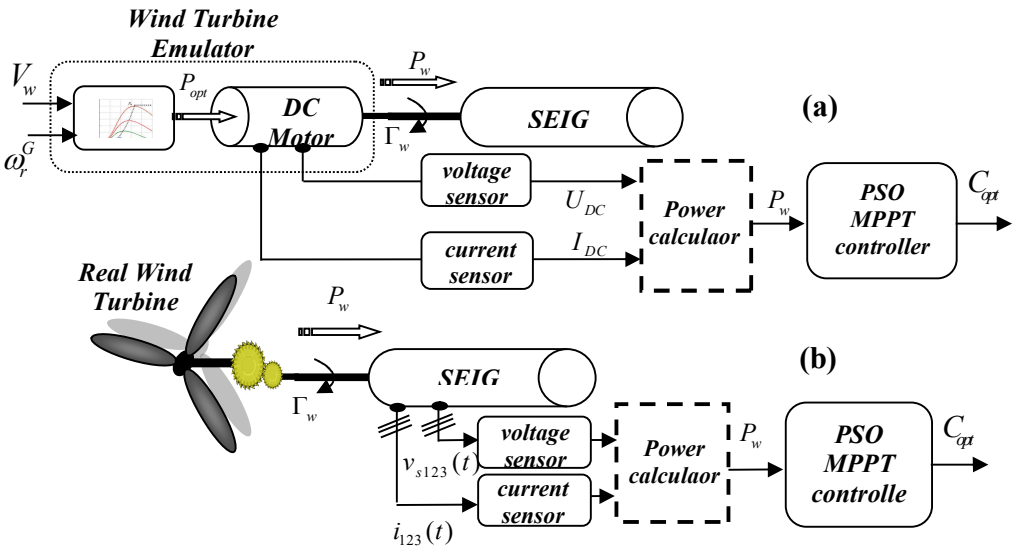

180
181 Fig. 4. Schematic diagram of power estimation: a) wind emulator and power estimation using DC motor
182 electrical signals b) power estimation using SEIG electrical signals.

In this case the losses are considered constants and the maxima values of electrical and mechanical powers obtained having the same optimal rotor speed value ω_{ropt}.

For experimental bench a realistic wind turbine curve and a rotor speed estimator are used to calculate the optimal reference mechanical power P_{opt} for the DC motor. It will be controlled under a PWM chopper to generate the corresponding mechanical power P_w to the SEIG shaft.

In the proposed PSO algorithm, as the rotor speed ω_r can be modified by changing the capacity value, a vector of capacitor C_j^k is used as initial value. j is the index of evolving parameters ($j = 1,2,...N_p$) called particles and their values change at each iteration k. For each iteration, these j values of the capacity are sent to the TCR system, which imposes to the SEIG a frequency f_j^k and a rotor speed ω_{rj}^k. The wind turbine emulator use a characteristic wind curve memorized in a look-up table and a rotor speed estimator to calculate P_{opt}. In the test bench is used a power loop control for DC motor under a PWM chopper to generate the corresponding mechanical power to the SEIG shaft. After the sending of the first capacity value C_j^k and the establishment of the permanent regime of mechanical and electrical quantities in the generator, voltage and current sensors are used to measure the electrical power and to estimate the mechanical power (P_{wj}^k) applied at the SEIG shaft. In the same iteration k the TCR system receives the second reference of the capacity value C_{j+1}^k, which imposes to the DC machine a new mechanical shaft power P_{wj+1}^k. The last value of the capacity for the iteration k is $C_{N_p}^k$. Each time necessary to establish the permanent regime and to measure electrical variables (U_{DC} and I_{DC}) for C_j^k depends on the global inertia system, parameters of the SEIG and requires for presented system

approximately 200 ms. For practical implementation the number of particles N_p must be limited ($N_p \le 4$). In presented application the global iteration time is near to 800 ms and this cycle will be repeated continuously until the real mechanical power achieves the maximum power points (MPP) . It can be noticed in Fig.4.b that for a real wind turbine the proposed PSO algorithm does not need to measure or estimate the rotor speed.

3.2. PSO Overview

The Particle Swarm Optimization (**PSO**) is a population-based searching algorithm. In general cases, it randomly produces N_p particles in searching space, where each particle is characterized by a position X_j^k in the searching space, and a velocity V_j^k [26, 28]. Each position of particle $X_j^{(k)}$ (in this case the capacity C_j^k) represents a solution of the problem and the "velocity" $V_j^{(k)}$ its displacement (variation of ΔC_j^k) in the searching space (between $C_{\min}$ and $C_{\max}$). The particles have memory to keeps track of its previous best particle called P_{best} which corresponds to an optimal fitness function Fit_{opt} (a mathematical function where the objective is to be minimized by changing the particles) obtained for iteration k. After the second iteration (k+1) is memorized (between P_{best_k} and $P_{best_{k+1}}$), the particle gives the minimized value of the Fit_{opt}. This particle (capacity in presented application) is called G_{best}. This concept considers a random weighted acceleration at each time step [28]:

$$\begin{cases} V_j^{(k+1)} = \mu V_j^{(k)} + \delta_1 rand[0,1](P_{best} - X_j^{(k)}) + \delta_2 rand[0,1](G_{best} - X_j^{(k)}) \\ X_j^{(k+1)} = X_j^{(k)} + V_j^{(k+1)} \end{cases} \quad (16)$$

where, $j = 1, 2, ...N_p$ is the index of particles, μ is the momentum or inertia ($\mu = 0.5$), δ_1 and δ_2 are a positive constant ($\delta_1 = \delta_2 = 0.5$), $rand$ is random numbers which are uniformly distributed in [0, 1],

and k is the iteration number. A typical movement of particles in the optimization process is shown in Fig. 5.

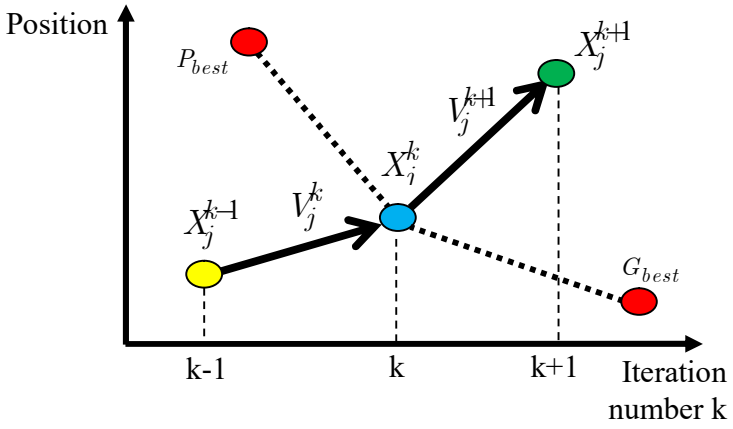

Fig. 5. Typical movement of particles in the searching space or optimization process.

In this figure the general spatial evolution case (between two iterations k, and k+1) of particles $X_j^{(k)}$ to $X_j^{(k+1)}$ is presented. It takes in consideration the velocity evolution from V_j^k to V_j^{k+1}. The best $X_j^{(k)}$ value for the j particles which give a minimal value for *Fit* function at iteration k is memorized with the name P_{best} (local best value) and the best value between all realized iterations is memorized with the name G_{best} (global best value). In the presented PSO algorithm a scalar particles evolution is considered where the particles are capacity values $(C_1^{(k)}, C_2^{(k)}, C_3^{(k)}, C_4^{(k)} \ldots)$ and the velocity evolution are the capacity variation $\Delta C_1^k, \Delta C_2^k, \Delta C_3^k, \Delta C_4^k \ldots.$

3.3. Application of PSO Algorithm for MPPT

In this paper, the initial N_p particles $(N_p = 4)$ are chosen to be uniformly distributed between $C_{\min}$ and $C_{\max}$. So, the value of particles and the corresponding velocity at the first iteration (k=1) are defined as:

$$X_j^{(k)} = V_j^{(k)} = C_j^k = \frac{C_{\max} - C_{\min}}{N_p - 1}(j-1) + C_{\min} \qquad (17)$$

$$j = 1, 2, \ldots N_p$$

where, for the presented algorithm, $C_{\min} = 35\mu F$ and $C_{\max} = 110\mu F$ are the low bound and the upper bound values of the optimal capacitor C_{opt}. The objective of the PSO algorithm is to maximize the generated power of the wind turbine ($P_w(C_j^{(k+1)}) > P_w(C_j^{(k)})$) consequently to minimize the fitness function Fit described by the following equation:

$$Fit = \min \Delta P = \left| P_{nom} - P_w(C_j^k) \right| \tag{18}$$

The updating of the particles $C_j^{(k)}$ and each capacity variation $\Delta C_j^{(k)}$, are given by the following equation [26]:

$$\begin{cases} \Delta C_j^{(k+1)} = \mu \Delta C_j^{(k)} + \delta_1 rand[0,1](C_{jPbest}^k - C_j^{(k)}) + \delta_2 rand[0,1](C_{jGbest}^k - C_j^{(k)}) \\ C_j^{(k+1)} = C_j^{(k)} + \Delta C_j^{(k+1)} \end{cases} \tag{19}$$

where, C_{jPbest}^k and C_{jGbest}^k are the local and global best capacity solution which lead to a minimal value of the Fit. The best local capacity solution is obtained using the following relationship:

$$C_{jPbest}^k = \begin{cases} C_j^k \text{ for } P_w(C_j^{(k)}) > P_w(C_{j-1}^{(k)}) \\ C_{j-1}^k \text{ for } P_w(C_j^{(k)}) < P_w(C_{j-1}^{(k)}) \end{cases} \tag{20}$$

At latest iteration k the best local power is obtained for the best capacity value:

$$P_w^k = P(C_{jPbest}^k) \tag{21}$$

For the global best capacity solution, considering all realized iterations C_{jGbest}^k is defined by the best solution under latest and previous iteration. It is given as:

$$C_{jGbest}^k = \begin{cases} C_{jPbest}^k \text{ for } P_w(C_{jPbest}^{(k)}) > P_w(C_{jPbest}^{(k-1)}) \\ C_{jPbest}^{k-1} \text{ for } P_w(C_{jPbest}^{(k-1)}) > P_w(C_{jPbest}^{(k)}) \end{cases} \tag{22}$$

This capacity C_{jGbest}^k gives the minimal value for fitness function at iteration k and it makes it possible to extract more power from the wind turbine. We note that, in order to avoid the disconnection of the

256 SEIG, limitations of the capacity value must be imposed ($C_{\min} < C_j^k < C_{\max}$). Taking this constraint into

257 consideration the new capacity can be expressed by:

258
$$C_j^{k+1} = \begin{cases} C_{\min} \text{ for } C_j^{(k)} + \Delta C_j^{(k+1)} < C_{\min} \\ C_j^{(k)} + \Delta C_j^{(k+1)} \text{ for } C_{\min} < C_j^{(k)} + \Delta C_j^{(k+1)} < C_{\max} \\ C_{\max} \text{ for } C_j^{(k)} + \Delta C_j^{(k+1)} > C_{\max} \end{cases} \quad (23)$$

259 Fig.6.a illustrates the application of the PSO algorithm in tracking the MPP, using a first vector of

260 capacitor with four particles. To start the optimization process (iteration k), the algorithm transmits to

261 the TCR system four capacitor reference values ($C_1^k, C_2^k, C_3^k, C_4^k$). The number of the particles must be

262 correlated with the system inertia and in this application limited to N_p=4. In Fig. 6.a, the four initial

263 particles are marked with circular points and for each point there is one capacitor value. Each capacitor

264 imposes a rotor speed ($\omega_{r1}^k, \omega_{r2}^k, \omega_{r3}^k, \omega_{r4}^k$) which corresponds to a mechanical power ($P_{w1}^k, P_{w2}^k, P_{w3}^k, P_{w4}^k$).

265 We can notice here that C_3^k is the best particle in the first iteration k, which gives the best power value (

266 $P_{best} = P_{w3}^k$), corresponding to maximum mechanical power at the first iteration.

267 For the second iteration (iteration k+1), the particle updating is realized using equation 17. It is

268 calculated new capacitor vector $C_1^{k+1}, C_2^{k+1}, C_3^{k+1}, C_4^{k+1}$. These new particles are marked with square points

269 in Fig. 6.a. A new best personal particle C_3^{k+1} is found and the best power is obtained at P_{w3}^{k+1}, which

270 corresponds to best rotor speed ω_{r3}^{k+1} . In fact, it is a global best ($C_{Gbest} = C_3^{k+1}$), which represents the best

271 particles between the latest and the previous iterations corresponding to the greater best power P_{w3}^{k+1} .

272 In the third iteration (iteration k+2), all capacitor particles $(C_1^{k+2}, C_2^{k+2}, C_3^{k+2}, C_4^{k+2})$ come near to MPP. In

273 the subsequent iteration, due to very low velocity, the value of the rotor speed $(\omega_{r1}^{k+2}, \omega_{r2}^{k+2}, \omega_{r3}^{k+2}, \omega_{r4}^{k+2})$ is

274 approaching to optimal rotor speed ω_{ropt} . Therefore, the wind turbine power will be maintained at the

275 maximum power (P_{MPP}), and the oscillation around it diminishes.

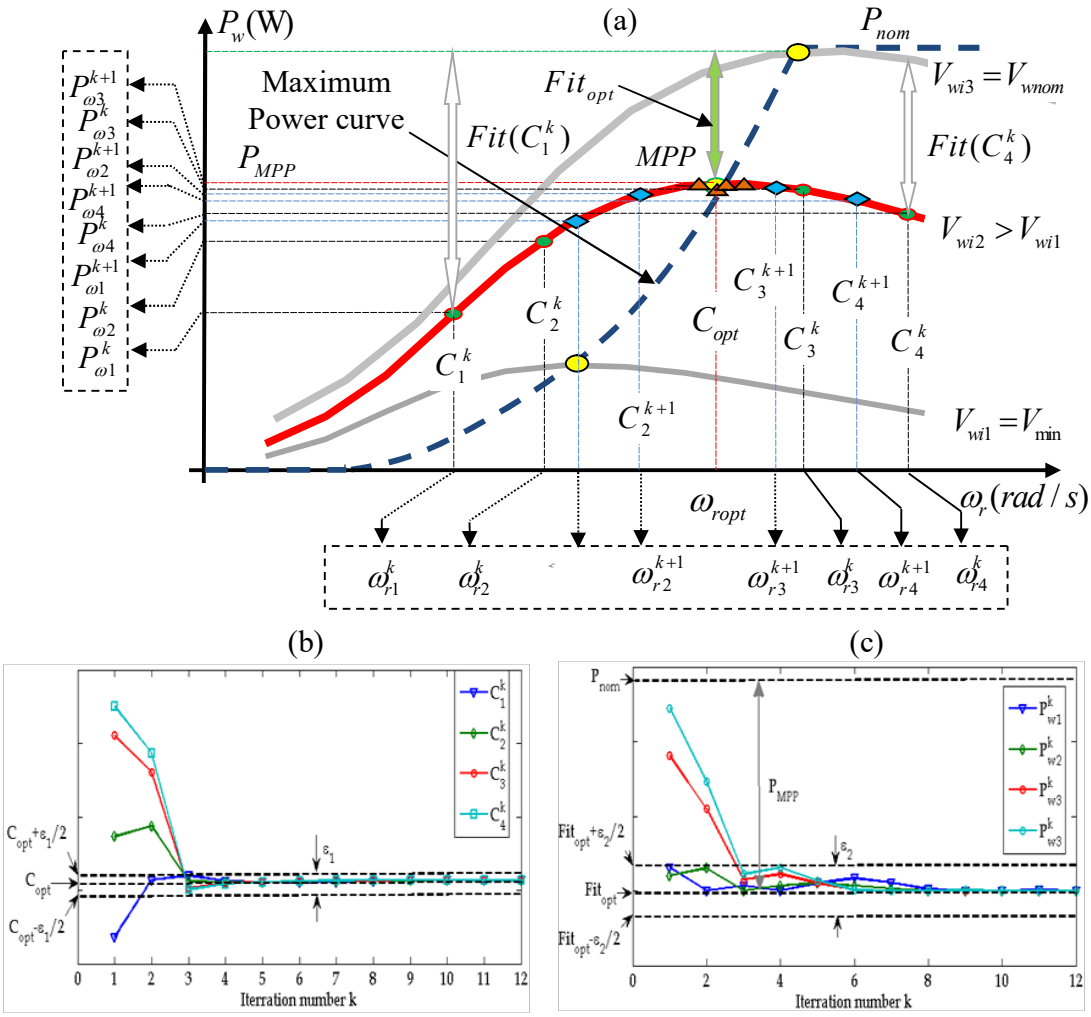

Fig. 6. Curves of a) MPP evolution on the wind turbine power, b) capacity and c) fitness optimization.

This sequence will be repeated continuously until the particles gradually come close to achieving MPP. This algorithm is realized during a constant wind speed. Fig. 6.b and Fig.6.c present the evolution of the capacity and fitness function for different iteration numbers. We can notice that after k=3 iterations the *Fit* is minimized and the turbine works at MPP. The time necessary to detect the MPP is dependent on the global system inertia of the machine. In presented test bench, the global time to detect the new MPP is estimated at approximately 2.4s (4x200 ms x3). If the wind speed applied changes the PSO algorithm must be reinitialized automatically to search again a new maximal power point. In this case two following simultaneous conditions must be respected to reinitialize the MPPT controller:

- particle convergence detection: $\left|C_j^{(k+1)} - C_j^{(k)}\right| < \varepsilon_1$

- sudden change in the fitness function. $\left|P_\omega(C_j^{k+1}) - P_\omega(C_j^k)\right| > \varepsilon_2$

Here the first condition imposes a small variation capacity between two iteration steps, error ε_1 and the second condition imposes a minimum power variation for a new "initialize particles" step, error ε_2. The flowchart of this algorithm is given in Fig. 7 where the delay time ΔT is estimated at 200 ms.

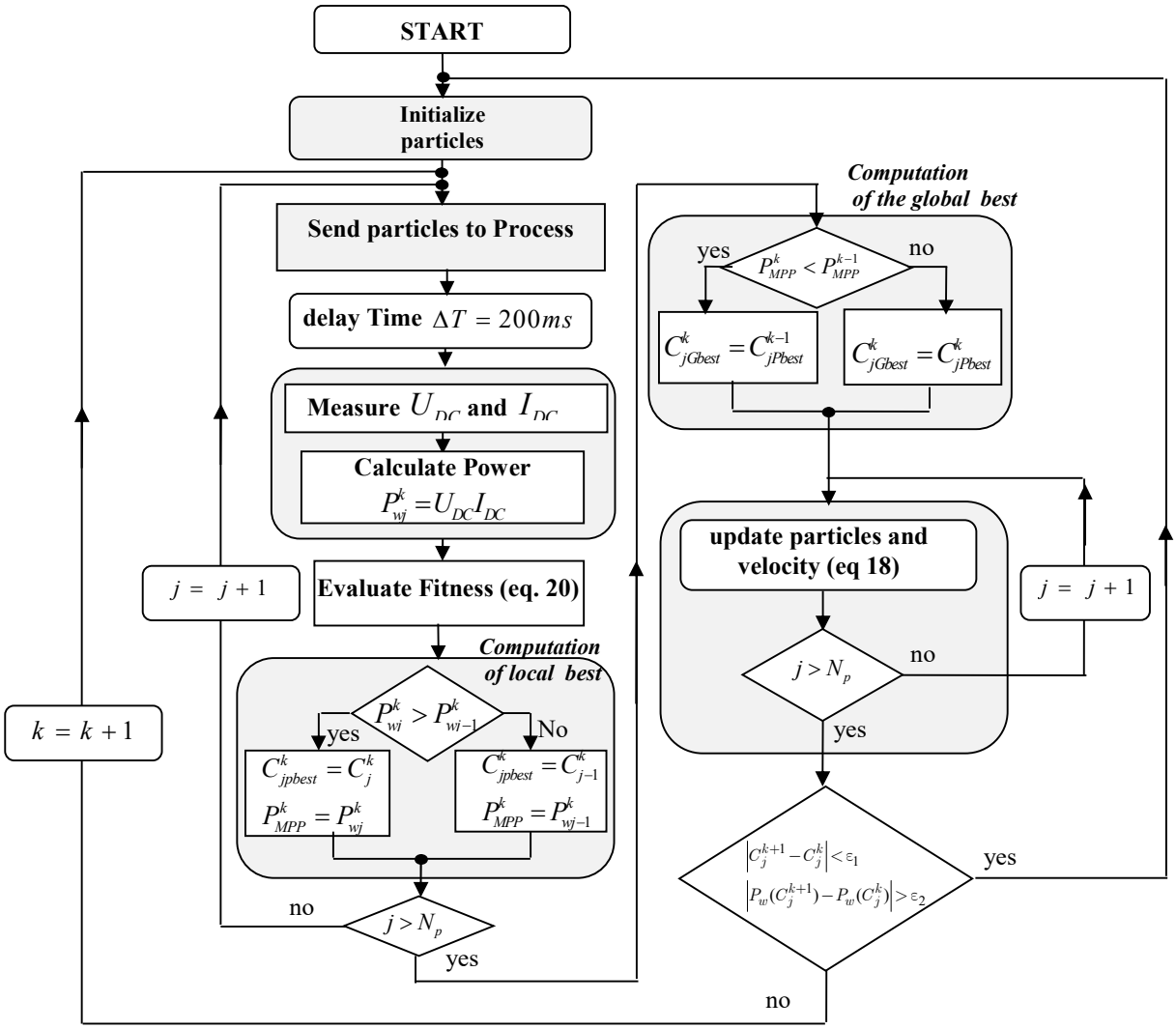

Fig. 7. Flowchart of PSO -MPPT proposed algorithm.

4. Simulation Results and Discussion

The simulations are carried out using Matlab/Simulink mathematical analysis software package. The system component parameters are presented in Appendix 1.

A TCR system composed of a fixed big capacitor $C_0 = 75\mu F$ and a fixed big inductance $L_0 = 335mH$ is used, whose principle is to adjust SEIG rotational speeds according to an optimal reference speed obtained from an MPPT controller. The simulink program begins with small initial voltage in the d and q axes of the stator due to residual magnetism. The block diagram of the global simulated system is shown in Fig. 8.

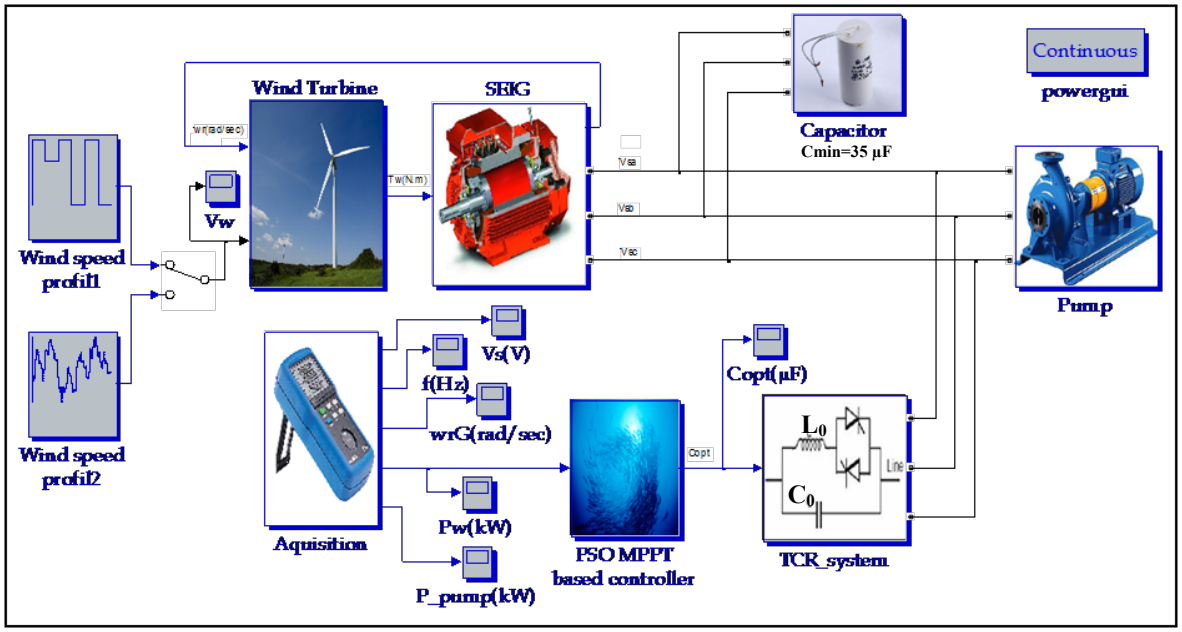

Fig. 8. Global simulink model for the wind turbine energy conversion system.

Initially, the SEIG start up process without pump, until the priming of the SEIG is reached. During this time, we hang the pump and the regulation system. Simulation was carried out for two wind speed profiles applied to the wind turbine, incorporating the proposed MPPT controller.

However, to validate the dynamic performance of the proposed MPPT controller, a step wind speed profile shown in Fig. 9 was applied to the wind turbine. In this case, the wind speed has been changed

311 from 13 m/s to 12 m/s and back to 13 m/s. The wind profile was to be changed again from 10 m/s to 13
312 m/s and back to 10 m/s.

313 The simulated waveforms of optimal capacitor, (C_{opt}), Fig. 10, rotor speed (ω_r^G) Fig. 11, shaft
314 power of wind turbine (P_w) Fig. 12 and pump (P_{pump}), wind turbine curve f(P_w, ω_r^G) Fig. 13
315 terminal RMS phase voltage (U_s) and frequency(f) Fig. 14 are presented for the step change of the
316 wind speed (V_w). It can be seen from Fig. 11 that the real rotor speed (ω_r^G) is converged to the optimal
317 rotor speed (ω_{ropt}^G) obtains by the PSO MPPT algorithm. Furthermore, the wind turbine power (P_w) is
318 maintained at the maximum power (P_{MPP}). In fact, the proposed MPPT controller has managed to track
319 the MPP for different values of wind speed (Fig. 13).

320 To observe the performance of the proposed MPPT algorithm, the instantaneous wave forms of the
321 first line voltage of the SEIG and those of the TCR system is shown and zoomed in Fig.15.

322 In Fig.16 the first line currents of the I_{SEIG}, the first line current I_{TCR} of the TCR system and those of
323 the pump are shown. We can notice that the I_{TCR} changing during each considered interval (V_w=12m/s,
324 V_w=10m/s, V_w=13m/s) when the reactive power is changed and so the ω_r respectively the frequency.

325 Furthermore, to assess the successful working of the proposed MPPT controller for a large value of
326 wind speed, a more realistic wind speed profile illustrated in Fig.17 was applied to the wind turbine.
327 Simulation results represent the optimal capacitor variation (C_{opt}). Fig. 18, the rotor speed (ω_r^G), Fig.
328 19 the active power of wind turbine (P_w), pump (P_{Pump}), estimation power by MPP algorithm P_{MPP}, Fig.
329 20, terminal RMS voltage (U_s) and frequency (f) Fig. 21, gives the time evolution of presented
330 parameters.

It can be seen from this figure that the maximum value of power of the turbine (P_w) shown in Fig.12 is already reached, and it was equal to the MPP power found by the MPPT controller. It can therefore be observed from the simulation results a good tracking capability of the proposed MPPT controller.

The first and the second test involve increasing or decreasing the reference speed keeping the torque constant. The aim of this case is to evaluate the performance of the proposed PSO-MPPT controller.

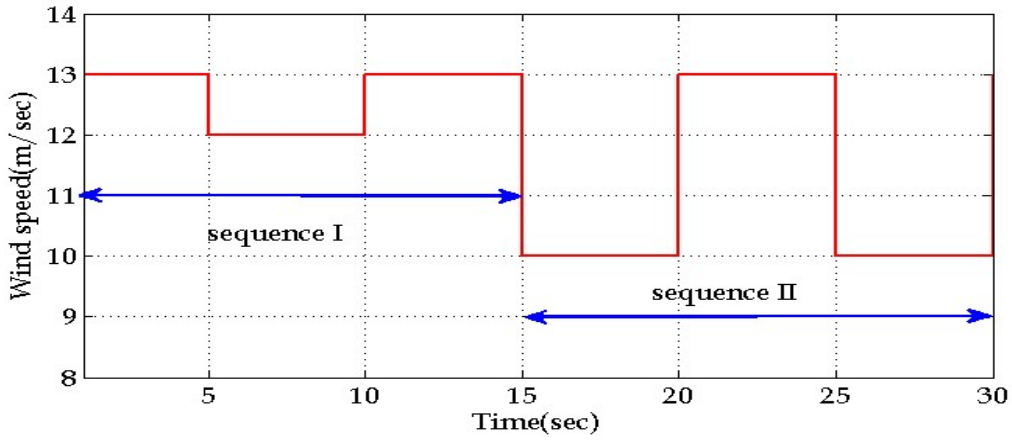

Fig . 9. Step wind speed profile for simulation tests.

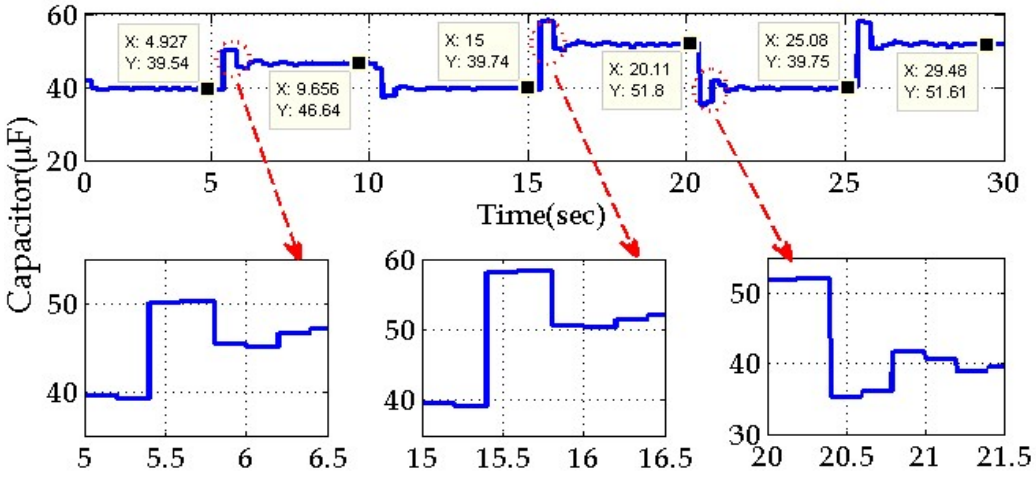

Fig. 10. Variations of optimal capacitor during step wind speed variation; V=13m/s and V=12m/s.

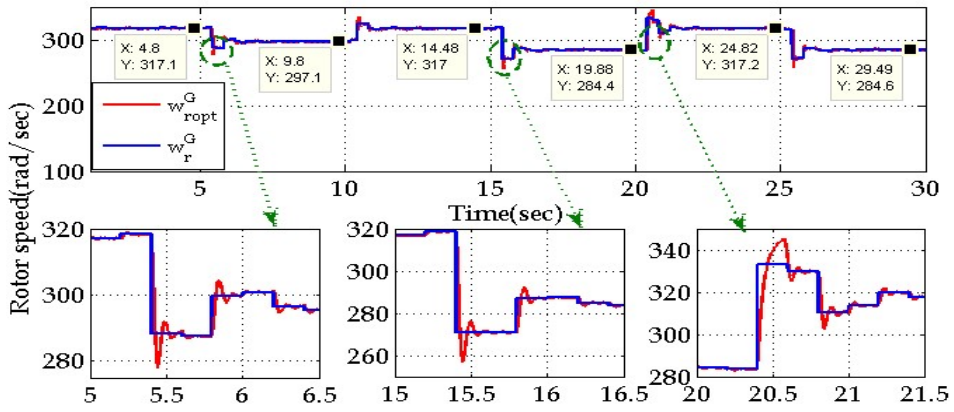

341 :

342 Fig. 11. Variations of optimal rotor speed and measured rotor speed during wind speed variation.
343

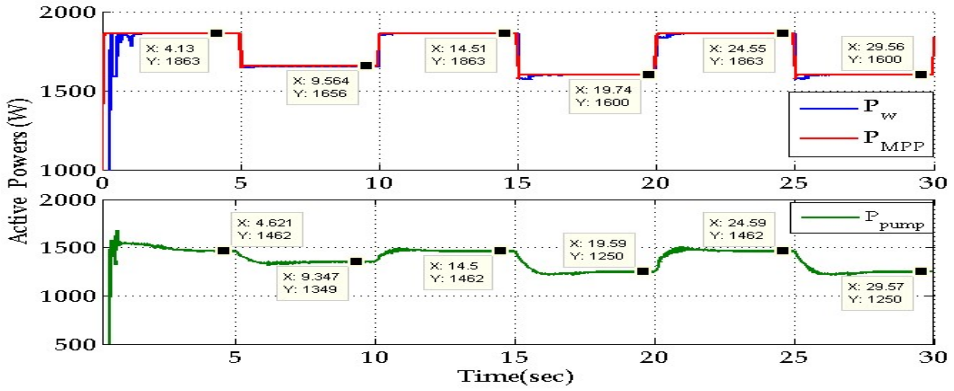

344

345 Fig. 12. Variations of active power of wind turbine P_w, active power of pump P_{pump} and estimated power
346 P_{MPP} during wind speed step variation.

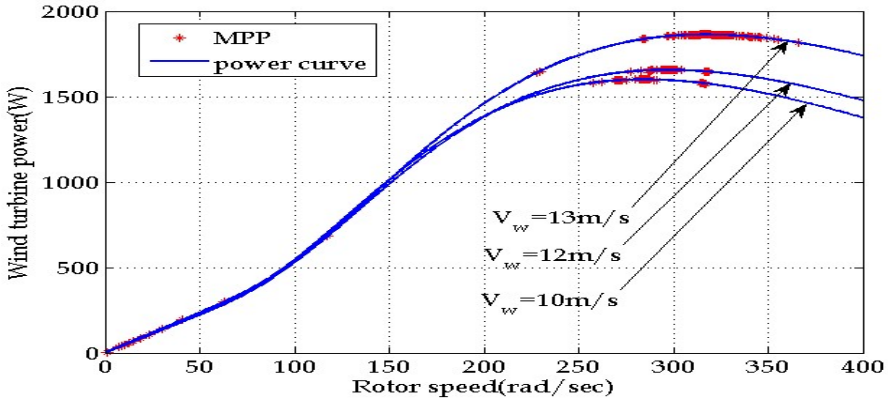

347

348 Fig. 13. Mechanical power of wind turbine characteristics and estimated power by MPP algorithm.

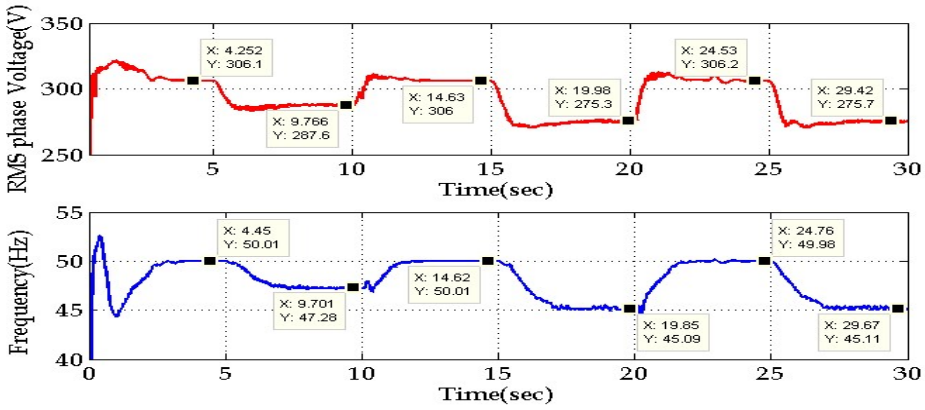

Fig. 14. Variations in RMS phase line voltage and frequency of the SEIG during wind speed step variation.

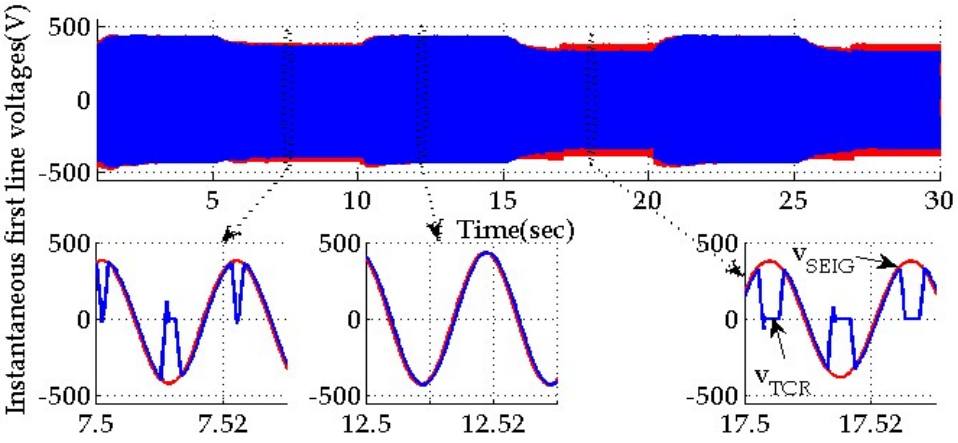

Fig. 15. Instantaneous first line voltage of the SEIG and TCR system during wind speed step variation.

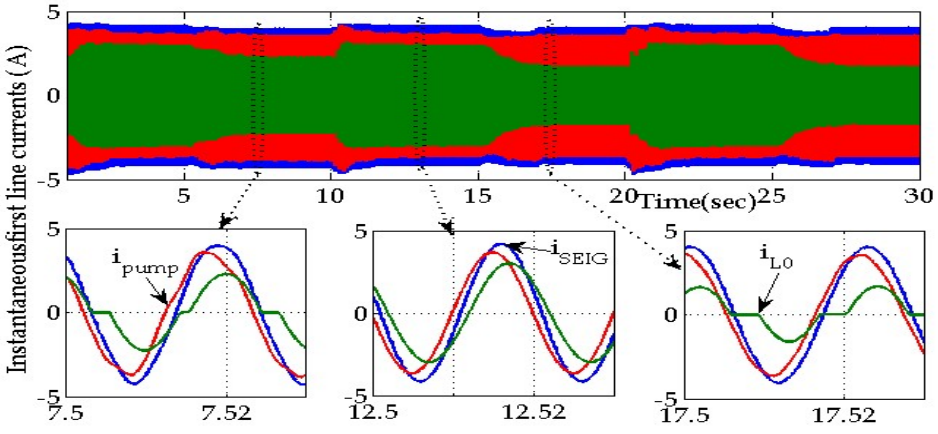

Fig. 16. Instantaneous first line currents of a) SEIG, b) TCR system and c) IM (pump) under wind speed perturbations.

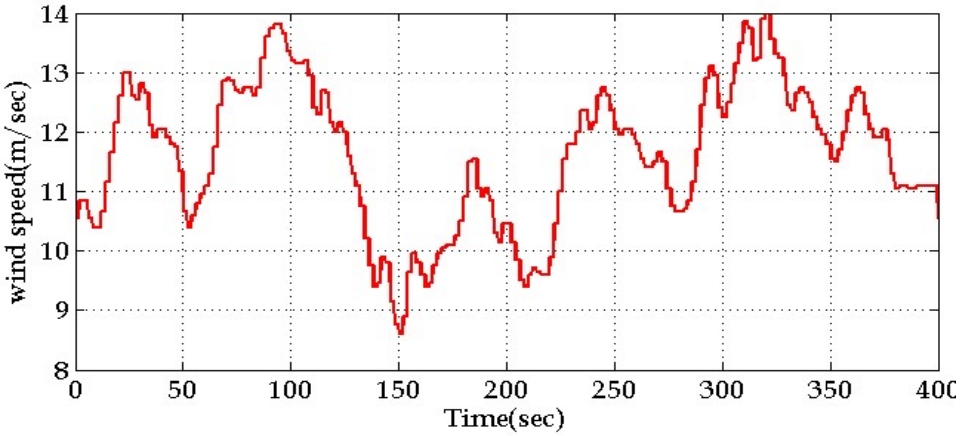

359

360 Fig. 17. Realistic wind speed profile used in the second simulation tests.

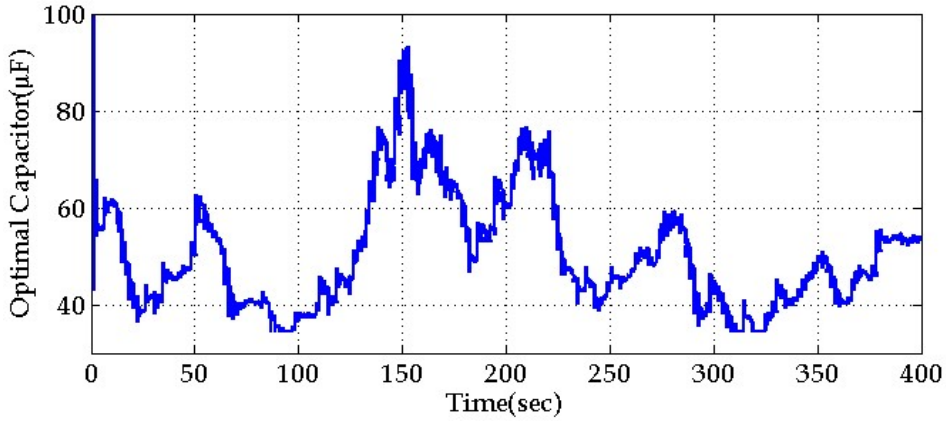

361

362 Fig. 18. Variations of optimal capacitor during wind speed variation.

363

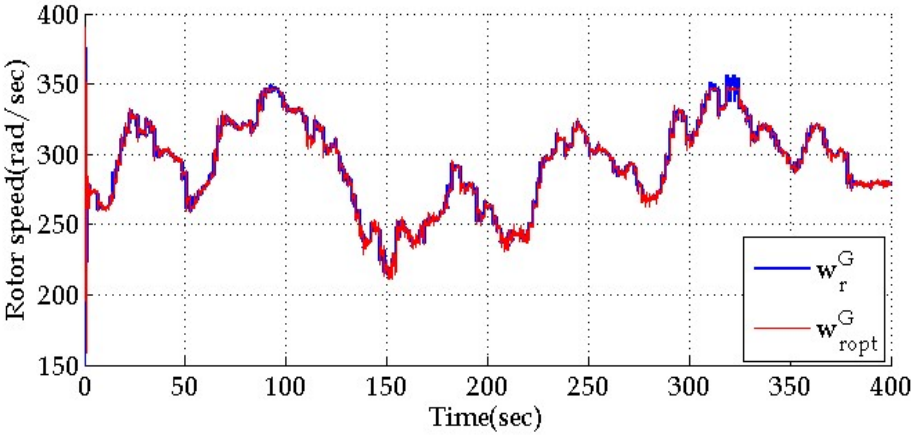

364

365 Fig. 19. Variations of optimal rotor speed and measured rotor speed during wind speed variation.

366

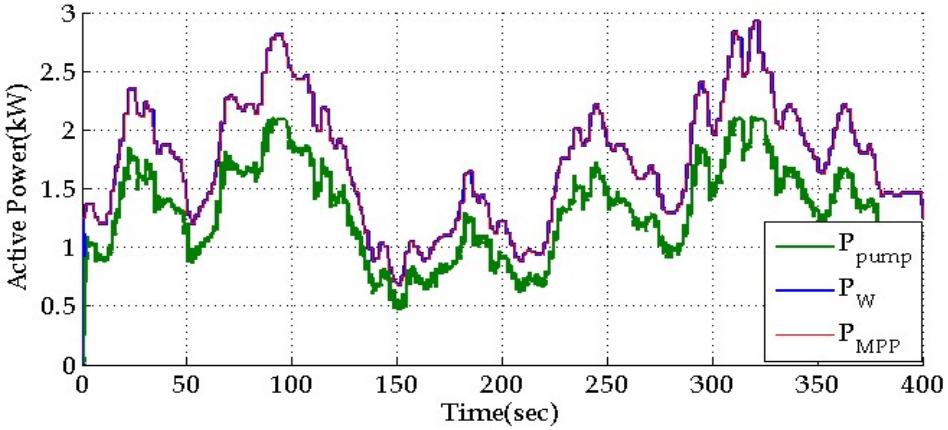

Fig. 20. Variations of wind turbine active power, active pump, and estimated power during wind speed variation.

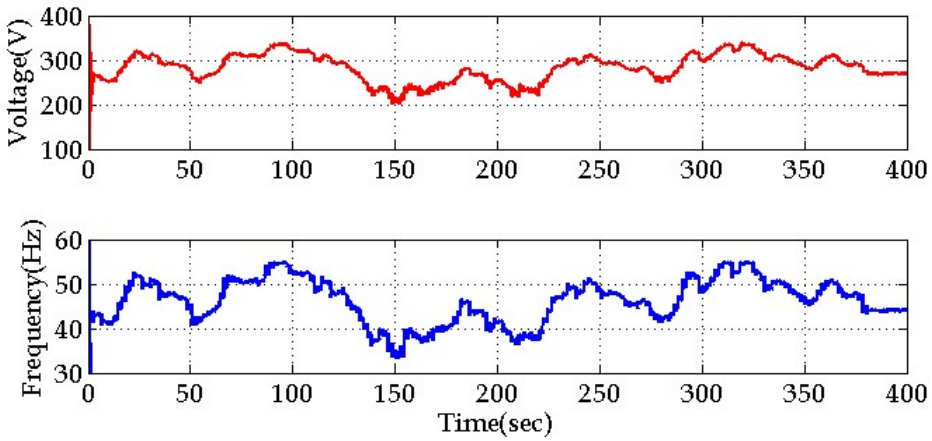

Fig. 21. Variations of line RMS voltage and frequency of the SEIG during wind speed variation.

5. Experimental Results and Discussion

5.1. Experimental Setup

The configuration of the experimental test bench is shown in Fig. 22. The proposed MPPT algorithm is implemented using a digital controller based on a dSPACE unit. The system components are:

- power-controlled DC motor drive which is used to emulate the characteristics of the wind turbine and to gives P_w at the SEIG shaft.
- 2[kW] squirrel-cage induction motor which is mechanically coupled to a break to emulate the centrifugal pump system, a TCR system converter connected in parallel with the SEIG output

terminals for the control of the reactive power, and a dSPACE controller board which is interfaced with a PC under Matlab/Simulink.

The output signals of the voltage and current transducers are sampled in dSPACE DSP under DS1104-ADC blocks. Low pass filters are used in measuring units to eliminate the unwanted high-frequency noise. The PWM pulses from the dSPACE are sampled under a DS1104-DSP-PWM block to generate standard 10 kHz fixed-frequency PWM pulses.

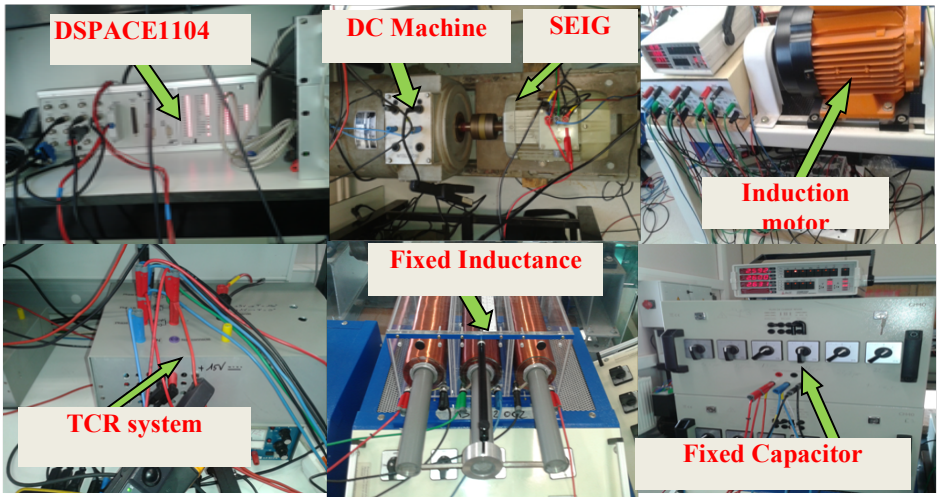

Fig. 22. Constituting elements of the experimental test bench.

5.2. Experimental Results

The performance of the MPPT control strategy was validated experimentally using a laboratory test bench composed of an IG which feeds an IM loaded by a specific break characteristic in order to assure a pump emulator. Different wind speed operating conditions are created by a DC motor which receives a power control in order to assure a constant power P_w at the SEIG shaft making it possible to investigate the dynamic characteristics of a SEIG-Pump system and to find the maximum of the power with the proposed method.

Experimental tests were carried out considering two speed profiles applied to the wind turbine, the first considers a decrease and the second an increase of the wind speed turbine. These profiles are used

403 to test the performances of the new proposed PSO MPPT controller algorithm and to analyze the signal
404 variations. During the tests, a step wind (power) variation is considered. The following tree pictures
405 (Fig. 23, Fig. 24 Fig. 25) shown the evolution of specific parameters during the decreasing wind speed.
406 As the frequency is dependent on the rotor speed the step reference is highlighted by the frequency
407 reference presented in Fig. 23. For experimental induction machines characterized by the parameters
408 presented in Appendix 1, the frequency 50 Hz corresponds to 13 m/s wind speed and the frequency 47.4
409 Hz to 12 m/ s wind speed. The transitory time includes the inertia of the SEIG-Pump system and also of
410 the wind turbine emulator which uses a power control loop.

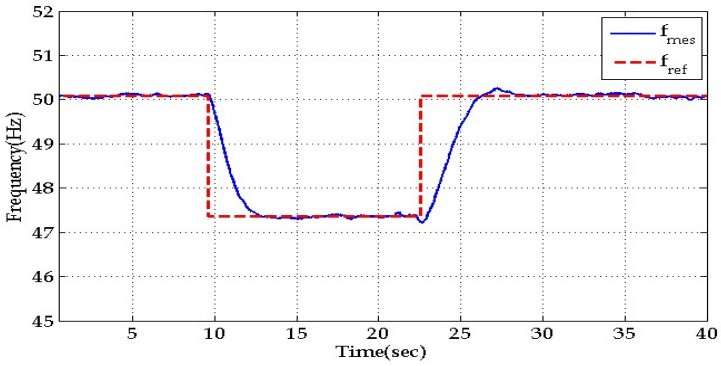

411

412 Fig. 23. Wave forms of reference frequency f_{ref} and SEIG measured frequency f_{mes} for wind speed
413 switching from V_w = 13m/s to V_w = 12 m/s and return to 13 m/s.
414
415 The reference power P_{ref} applied at the SEIG, the estimated power obtained from PSO algorithm and
416 a power consumed by the pump P_{pump} are shown in Fig. 24. For MPP reaching an adjustment of the
417 SEIG excitation capacitor is applied using a TCR system. We can notice a good power estimation
418 obtained by the proposed algorithm compared to P_w power reference applied to the PWM converter
419 (Fig.1). The difference between P_{pump} and P_w corresponds to the DC motor and IG losses.

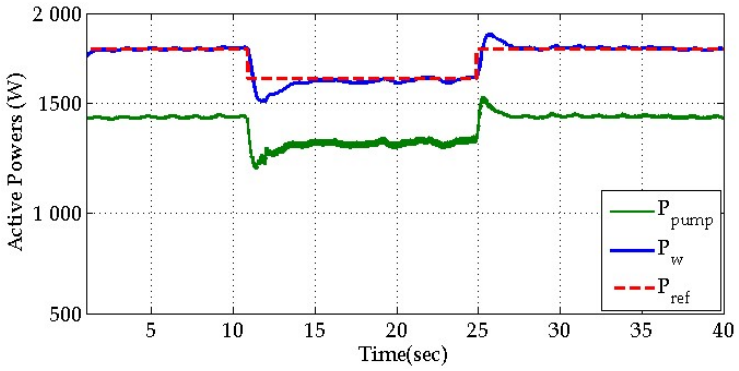

Fig. 24 . Wave forms of reference power P_{ref} , estimated power P_w obtained by PSO-MPP algorithm and the power consumed by the pump P_{pump} for wind speed switching from V_w = 13m/s to V_w = 12 m/s and return to 13 m/s.

The RMS voltage variation measured at the SEIG output is presented in Fig. 25. Here during the wind variation the voltage changes between 308V at 284V with the low overtaking caused by the wind power variation (regulation) at the SEIG shaft.

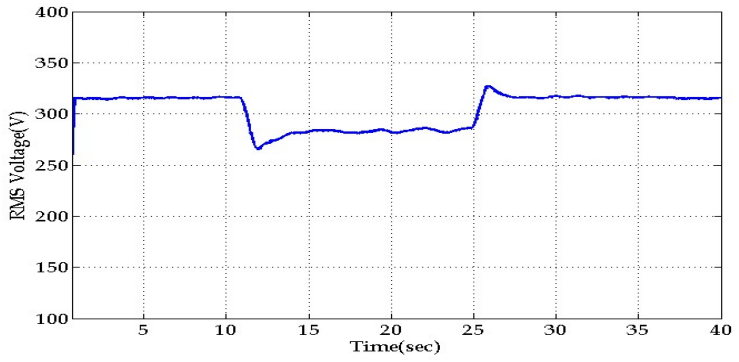

Fig. 25. Measured phase RMS voltage at the SEIG output for wind speed switching from V_w = 13m/s to V_w = 12 m/s and return to 13 m/s.

For considered speed (power) variation the wave forms of recording signals are presented in Fig. 26. Here the top recording lines show the voltage and the current measured at the SEIG output and the bottom lines the voltage and the current measured at the TCR input. We can notice the voltage decreasing with a very low influence of the currents.

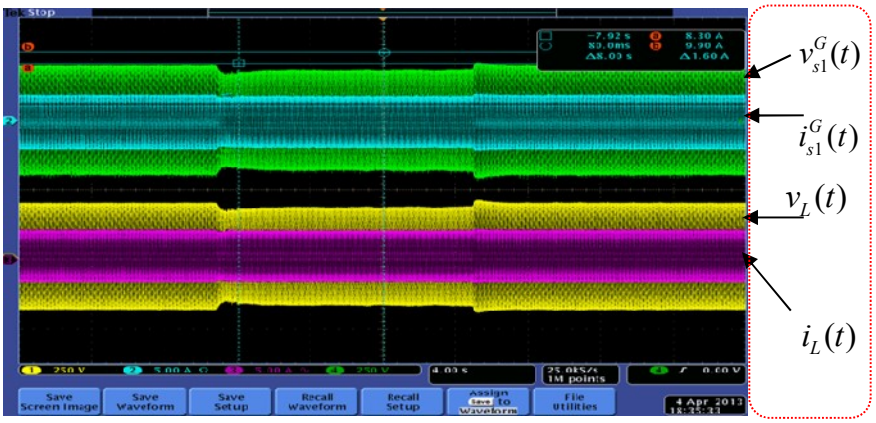

Fig. 26. Wave forms of recording signals : top lines show voltage and current lines measured at the SEIG output, bottom lines show voltage and current lines of TCR system for wind speed switching from V_w = 13m/s to V_w = 12 m/s and return to 13 m/s.

The following tree pictures show the signal variations (frequency, power, voltage,) in the second case when the wind speed increases from V_w = 10m/s to V_w = 13 m/s and returns to 10 m/s. The frequency target and the real frequency variations are presented in Fig. 27. We can notice in this case a frequency value close to the reference with different transitory interval time for increasing and decreasing of the wind speed.

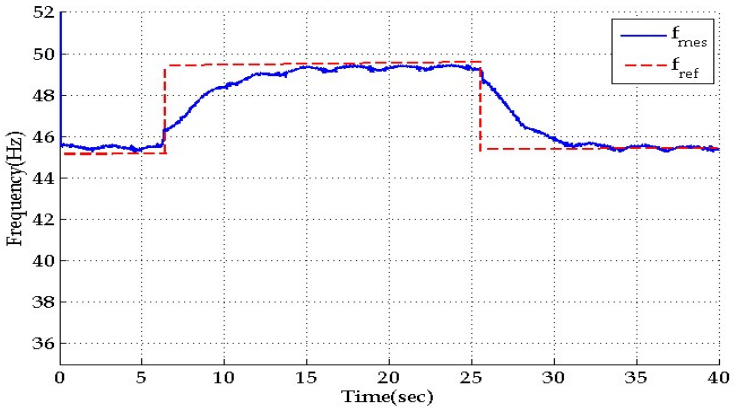

Fig. 27. Wave forms of reference frequency f_{ref} and SEIG measured frequency f_{mes} for wind speed switching from V_w = 10m/s to V_w = 13 m/s and return to 10 m/s.

For this case the power estimation P_{MPP} obtained by the proposed algorithm and the measured power absorbed by the pump P_{pump} are presented in Fig. 28. The reference power P_{ref} is a step signal changing

between 1640W and 1870W. Taking into consideration the DC motor and the IG losses we can notice the identical variation for P_{pump} and P_{MPP}. The difference during the transitory interval between P_{MPP} and P_w can be justified by regulation power at the SEIG shaft.

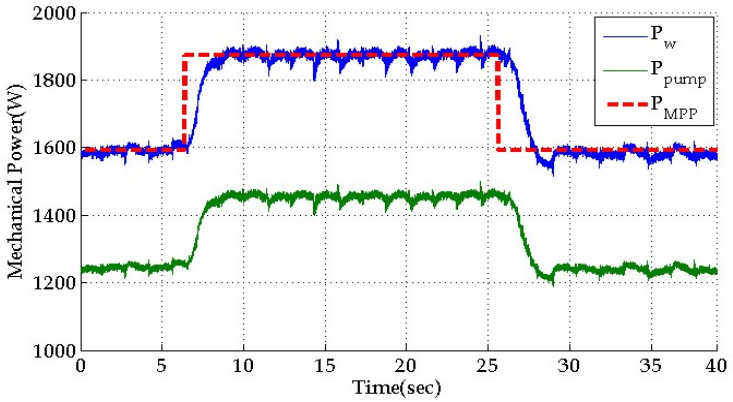

Fig. 28. Wave forms of reference power P_{ref}, estimated power P_w obtained by PSO algorithm and the power consumed by the pump P_{pump} from V_w = 10m/s to V_w = 13 m/s and return to 10 m/s.

The variation of the RMS voltage measured at the SEIG output for wind speed switching from V_w = 10m/s to V_w = 13 m/s and return to 10 m/s is presented in Fig. 29. Here during the steady state the voltage takes the values 278V and 308V respectively.

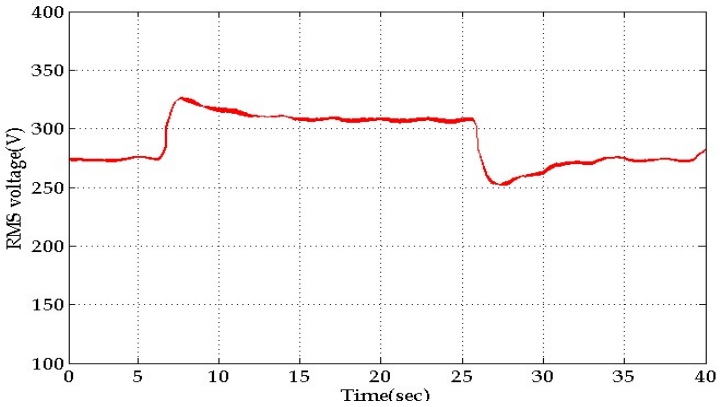

Fig. 29. Wave forms of the SEIG RMS voltage for wind speed switching from V_w = 10m/s to V_w = 13 m/s and return to 10 m/s.

In the presented figures (Fig. 28 and Fig. 29) the P_{pump} and RMS voltage are reconstituted signals obtained from instantaneous recording signals of current and voltage measured at the SEIG output and the P_w is the estimated power obtained by the proposed the PSO algorithm. The wave forms of recorded signals are presented in Fig. 30.

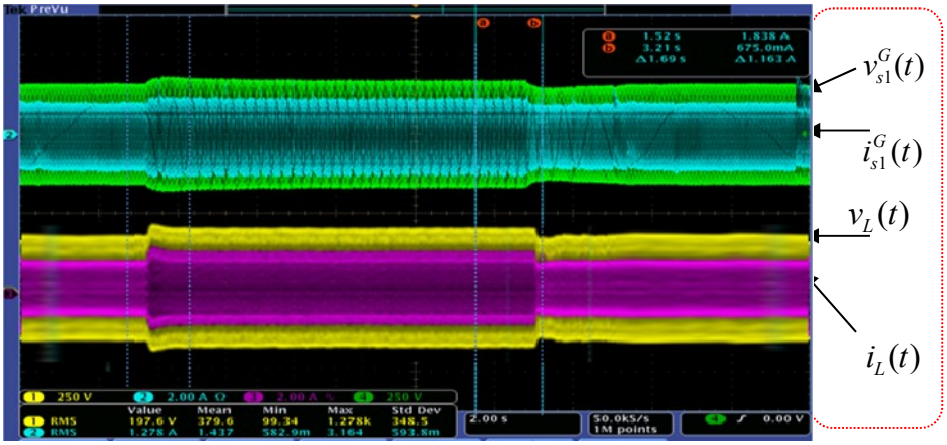

Fig. 30 . Wave forms of recording signals : top lines show voltage and current lines measured at the SEIG output, bottom lines show voltage and current lines of TCR system for wind speed switching from V_w = 10m/s to V_w = 13 m/s and return to 10 m/s.

We can observe in Fig. 30 an increasing of the voltage and the current signals (top lines) for V_w = 13 m/s and a increase of the I_L current consumed by inductance L_0 in order to decrease the reactive power in the system. For the second case considered the wave forms of the current and voltage signals are presented in the following pictures. Fig. 31 gives the signals for wind speed V_w=10m/s and Fig. 32 for V_w=13m/s.

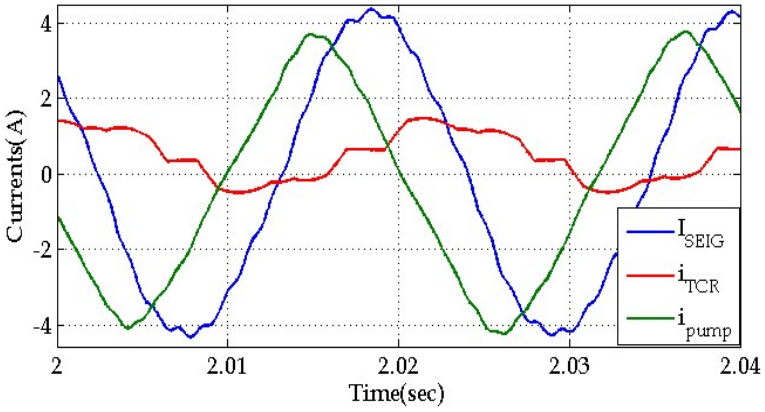

a) I_{SEIG} current, I_{pump} current and I_{TCR} current

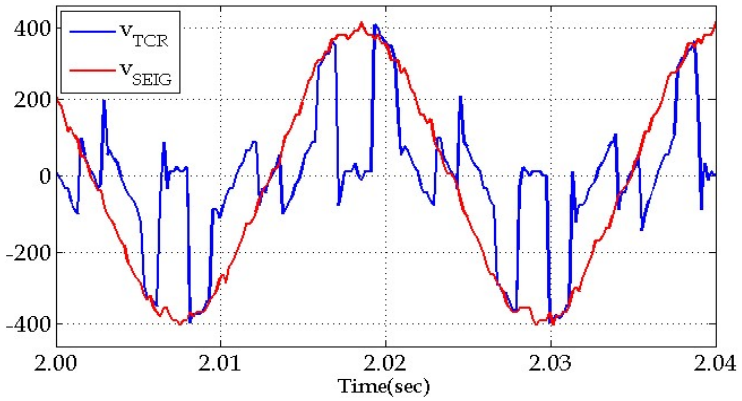

476

477 b) first line voltage of SEIG, and first line voltage of TCR system

478 Fig. 31. Zoomed wave forms of a) current and b) voltage for V_w=10m/s wind speed.

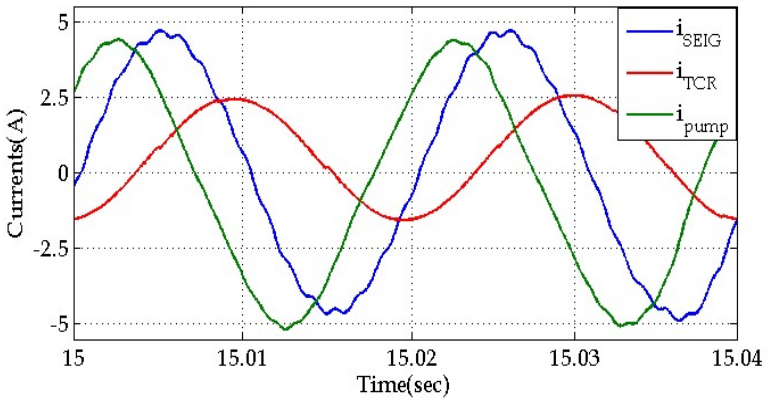

479

480 a) I_{SEIG} current, I_{pump} current and I_{TCR} current

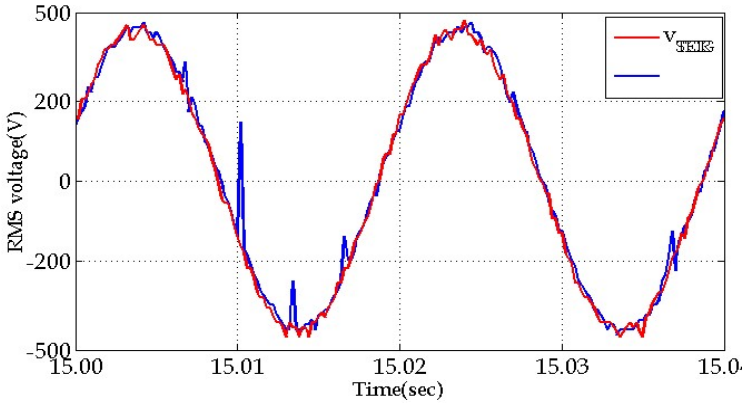

481

482 b) first line voltage of SEIG, and first line voltage of TCR system

483 Fig. 32. Zoomed wave forms of a) current and b) voltage for V_w=13m/s wind speed.

To conclude all steady state analyses results, a summary of the SEIG performance is tabulated in Table 1.

Tab.1 Steady state results

	Simulation Results			Experimental Results		
V_w(m/s)	**12**	**10**	**13**	**12**	**10**	**13**
V_s(V)	**285.5**	**274.4**	**303**	**284**	**278**	**308**
f(Hz)	**47**	**45**	**50**	**47.4**	**45.1**	**50**
P_{MPPT}(W)	**1660**	**1598**	**1880**	**1640**	**1580**	**1870**
P_{Pump}(W)	**1352**	**1250**	**1462**	**1335**	**1247**	**1460**
Losses(W)	**308**	**348**	**418**	**305**	**333**	**410**
η (%)	**81.5**	**78.2**	**77.7**	**81.4**	**78.9**	**78**

6. Conclusion

This paper presents the performance of a Self Excited Induction Generator Pumping system used in the case of variable wind speed. The system is able to track a maximum power using a generated power as input. The Maximum Power Point Tracking controller sets the generator to work at the optimal rotor speed command, which is achieved through a frequency control loop by changing the reactive power. The proposed system has been implemented in a real-time application, using two Induction Machine (generator and pump) and a DC motor for emulator of the wind turbine behavior. Simulation and experimental results show the appropriate behavior of the system.

In this paper a new MPPT control algorithm involving PSO technique without use of a rotor speed sensor is proposed. The wind turbine in operation delivers the maximum mechanical output power for a given wind velocity. It is considered that the slip of the SEIG is very small. Therefore, when operating

499 the induction generator with wide rotor speeds achieving MPPT, the frequency of the SEIG is controlled
500 to reach the optimal rotor speed ω_{ropt} .

501 A proposed PSO-MPPT based algorithm is presented in this work as a case study. The advantage of
502 the proposed method is that it does not require the knowledge of wind speed, air density or turbine
503 parameters. The MPPT controller generates at its output the optimum capacitor command C_{opt} for rotor
504 speed control loop using only the instantaneous active power as input signal.

505 From, the analyses results, the PSO based MPPT has been proved to be useful in tracking the
506 maximum power point and it is able to respond to the changes of wind speed and power coefficients.

507 However, the global time for tracking of the MPP is dependent by the global inertia of the system
508 and SEIG parameters and can take few second time delay.

509 **Nomenclature**

Variable	Designation	Variable	Designation
A	Area swept by blades	l_s^G and l_s^M	Leakage inductance of the stator winding of IG and IM
B	Fundamental frequency susceptance		
C_0	Big fixed capacitor	l_r^G and l_r^M	Leakage inductance of the rotor copper of IG and IM
$C_{\min}$ and $C_{\max}$	Low bound and upper bound values of the optimal capacitor	L_m^G and L_m^M	Magnetizing inductances of the IG and IM
C_j^k	jth capacitor at iteration k	L_0	Big fixed self inductance.
C_{Gbest}	Global best capacitor of each group	N_p	Number of particles
C_{opt}	Optimal capacitor	p	Pair of poles
C_p	Power coefficient of the wind turbine	P_{jref}^k	jth reference mechanical power at iteration k
C_{pbest}^k	Best capacitor of jth particle until iteration k	P_{wj}^k	jth mechanical power at iteration k
f_j^k	jth frequency at iteration k	P_w, P_{pump}	Mechanical powers of the wind turbine respectively the pump
Fit , Fit_{opt}	Fitness function and Optimal Fitness function	P_{MPP}	Maximum power extracted from the wind turbine
G_{best}	Global best particles	P_{best}	Local best particles
j	Index of particles	Q_{TCR} , Q_{C0} and Q_L	Reactive powers of the TCR system, the capacitor and the inductance
J	Global inertia of system.	R_w	Radius of the wind turbine blade

k	k^{th} iteration	$rand$	Random numbers which are uniformly distributed in interval [0, 1]
k_n	Torque-rotor speed coefficient	U_{DC} and I_{DC}	DC voltage and current
V_j^k	Velocity of jth particles at iteration k	δ_1 and δ_2	Positive constants
V_w	Wind speed	λ_{opt}	Optimum Tip Speed Ratio.
V_s	RMS of the SEIG terminal voltage	λ	Tip Speed Ratio.
X_j^k	Position of j^{th} particles at iteration k	μ	Momentum or inertia
β	Blade pitch angle	ω_r^G and ω_r^M	Electrical rotor speed of IG and IM
Γ_{em}^G and Γ_{em}^M	Electromagnetic torque developed by the IG and IM	ω_{rj}^k	j^{th} rotor speed at iteration k
Γ_f	Friction torque	ω_{ropt}	Optimum rotor speed
Γ_w	Mechanical torque of the wind turbine	ω_{ropt}^G	Optimal rotor speed

Appendix 1

The considered induction generator is characterized by:

$380/660V$, $7.3/4.2A$, $1420\ rpm$, $f=50Hz$, $\cos(\varphi)=0.8$, $p=2$, $R_s^G=8.66\ \Omega$, $R_r^G=3\ \Omega$,

$l_s^G=24.24\ mH$, $l_r^G=36.3\ mH$, $L_m^G=534\ mH$, $L_s^G=558.24\ mH$, $L_r^G=570.3\ mH$, $\Gamma_f=1.3N.m$

The considered induction motor is characterized by:

$380/660V$, $5.2/3A$, $1420\ rpm$, $f=50Hz$, $\cos(\varphi)=0.89$, $p=2$, $r_s^M=3.7\ \Omega$, $r_r^M=2.72\ \Omega$,

$l_s^M=20.78\ mH$, $l_r^M=14.8\ mH$, $L_m^M=436.6\ mH$, $L_s^M=457.38\ mH$, $L_r^M=451.4\ mH$,

References

[1] R. C. Bansal, "Three-phase Self-Excited Induction Generators: an overview," 16th national power systems conference, IEEE transactions on Energy Conversion, vol. 20, no. 2, June 2005, pp. 292-299.

[2] D. Halamay, T. Brekken, A. Simmons, and S. McArthur, "Reserve Requirement Impacts of Large-Scale Integration of Wind, Solar and Ocean Wave Power Generation, " IEEE Transactions on Sustainable Energy, no 2, Dec 2011, pp. 321-328.

525 [3] L. Wang, and Z. Chen, “Stability Analysis of a Wave-Energy Conversion System Containing a Grid-
526 Connected Induction Generator Driven by a Wells Turbine,” IEEE Transactions on Energy
527 Conversion, no 25, Jun 2010, pp. 555-563.

528 [4] G. Ofualagba, E.U.Ubeku, “The analysis and modelling of a self-excited induction generator driven
529 by a variable speed wind turbine,” Federal University of Petroleum Resources, Effurun, Nigeria. In
530 Book –Fundamentals and Advanced Ttopics in Wind Power, Vol. 2, June 2011, ISBN 978-953-307-
531 508-2.

532 [5] I. Boldea, and S. Nasar, “The induction machine handbook. 1st ed. Boca Raton » USA: CRC Press;
533 2002.

534 [6] R. C. Bansal, T. S. Bhatti, and D. P. Kothari, “A bibliographical survey on induction generators for
535 application of nonconventional energy systems,” IEEE Trans. Energy Convers., Vol. 18, no. 3,
536 September 2003, pp. 433–439.

537 [7] Jayanta K. Chatterjee, “Analysis Voltage and Frequency Control of a Stand Alone Brushless Wind
538 Electric Generation Using Generalized Impedance Controller,” IEEE Trans. Energy Convers., vol.
539 23, no. 2, June 2008, pp. 632-641.

540 [8] J.F. Brudny, R. Pusca, and H. Roisse, “Wind turbines using self-excited three-phase induction
541 generators: an innovative solution for voltage-frequency control,” Eur. Phys. J. Appl. Phys. 43,
542 2008, pp. 173–187

543 [9] Bhim Singh, S. S. Murthy, Raja Sekhara , “STATCOM-Based Controller for a Three-Phase SEIG
544 Feeding Single-Phase Loads” IEEE Trans. Energy Convers., Vol. 29, no. 2, June 2014, pp. 320-331.

545 [10] S.S. Murthy, Bhim Singh, V. Sandeep, "An analytical performance comparison of two winding
546 and three winding single phase SEIG", Electric Power Systems Research, Vol. 107, February 2014,
547 pp. 36–44.

548 [11] Cosmas .U. Ogbuka, Member, IAENG and Marcel. U. Agu, MIEEE, “A Modified Approach to
549 Induction Motor Stator Voltage and Frequency Control,” Proceedings of the World Congress on
550 Engineering, 2011, Vol II, WCE 2011, 6 – 8 July 2011, London, U.K. pp. 978-988.
551 [12] Jayanta K. Chatterjee, “Analysis Voltage and Frequency Control of a Stand Alone Brushless
552 Wind Electric Generation Using Generalized Impedance Controller,” IEEE Trans. Energy Convers.,
553 vol. 23, no. 2, June 2008, pp. 632-641.
554 [13] Manel Ouali, Mohamed Ben Ali Kamoun, Maher Chaabene “ Investigation on the Excitation
555 Capacitor for a Wind Pumping Plant Using Induction Generator,” Smart Grid and Renewable
556 Energy, 2011, 2, pp. 116-125.
557 [14] Messaoud Makhlouf, Feyrouz Messai and Hocine Benalla “Vectorial Command Of Induction
558 Motor Pumping System Supplied By A Photovoltaic Generator,” Journal of Electrical Engineering,
559 Vol. 62, No. 1, 2011, pp. 3–10.
560 [15] V. Agarwal, R.K. Aggarwal, P. Patidar, C. Patki, A novel scheme for rapid tracking of maximum
561 power point in wind energy generation systems, IEEE Trans. Energy Convers. Vol. 25 , Jun 2010,
562 pp. 228-236.
563 [16] T. Ouchbel , Smail Zouggar, M.L. Elhafyani, M. Seddik, M. Oukili and A. Aziz “Power
564 maximization of an asynchronous wind turbine with a variable speed feeding a centrifugal pump,”
565 Energy Conversion and Management, Vol. 78, February 2014, pp. 976–984.
566 [17] David Laraa, Gabriel Merinoa, Lautaro Salazar, “Power converter with maximum power point
567 tracking MPPT for small wind-electric pumping systems,” Energy Conversion and Management, V.
568 97, June 2015, pp. 53–62.
569 [18] René Aubréea, b, François Augera, Michel Macéc, Luc Lorona, “Design of an efficient small
570 wind-energy conversion system with an adaptive sensorless MPPT strategy", Renewable Energy,
571 Vol. 86, February 2016, pp. 280–291.

572 [19] Dalala Z. M., Zahid Z.U., Wensong Y.U., Younghoon Cho, Gih-Sheng Lai, "Design and
573 Analysis of an MPPT Technique for Small-Scale Wind Energy Conversion Systems", IEEE Trans.
574 Energy Convers, Vol. 28, No. 3, September 2013, pp 756-767.
575 [20] Cong-Hui Huang, " Modified Neural Network for Dynamic Control and Operation of a Hybrid
576 Generation Systems, "Journal of Applied Research and Technology, Vol. 12, December 2014, pp.
577 1154-1164.
578 [21] David Lara, Gabriel Merinoa, Lautaro Salazar, "Power converter with maximum power point
579 tracking MPPT for small wind-electric pumping systems", Energy Conversion and Management, V.
580 97, June 2015, pp. 53–62.
581 [22] Samira Chekkal "Fuzzy logic control strategy of wind generator based on the dual-stator
582 induction generator", International Journal of Electrical Power & Energy Systems, Vol. 59, July
583 2014, pp. 166–175.
584 [23] A. Betz, Das Maximum der theoretisch möglichen Ausnutzung des Windesdurch Windmotoren,
585 Gesamte Turbinenwesen , Vol. 17, Jun 1920, pp. 307–309.
586 [24] J.G. Slootweg, S.W.H. de Haan, H. Polinder, W.L. Kling, "General model for representing
587 variable speed wind turbines in power system dynamics simulations", IEEE Trans. Power Syst. Vol.
588 18 , Decmber 2003, pp. 144-151.
589 [25] Ouchbel T, Zouggar S, Sedik M, Oukili M, Elhafyani M, et al. Control of the output voltage of
590 asynchronous wind turbine with variable speed using a static VAR compensator (SVC) smart
591 innovation, systems and technologies. Sustain Energy Build Part 1 , Vol. 12, March 2012, pp 17–30,
592 [26] Shi, Y., Eberhart, R.: "Empirical study of particle swarm optimization", Proceedings of the IEEE
593 Congress on Evolutionary Computation, Piscataway, NJ, IEEE Press , Jun 1999, pp 1945–1950.

[27] Ali Ajami and Mehdi Armaghan, “Application of Multi-Objective PSO Algorithm for Power System Stability Enhancement by Means of SSSC,” International Journal of Computer and Electrical Engineering, Vol. 2, No. 5, October 2010, pp. 838-845.

[28] Sabine Helwig, Frank Neumann, and Rolf Wanka, “Particle Swarm Optimization with Velocity Adaptation,” International Conference on Adaptive and Intelligent Systems. 24-25 September 2009, Las Vegas, pp.146-151.